Electronic Supplementary Material (ESI) for Materials Advances.

Supporting Information

Oxygen Reduction Reaction Catalyzed by Carbon Composites with Ruthenium-Doped Iron Oxide Nanoparticles

Qiming Liu,[a] Hong Bo Zhou,[a,b] Forrest Nichols,[a] Han-Lin Kuo,[c] Rene Mercado,[a] Bingzhang Lu,[a] Weiya Zhu,[a] Yashu Liu,[a,d] Jennifer Q. Lu,[c] Frank Bridges,[e] Shaowei Chen*,[a]

[a] Department of Chemistry and Biochemistry, University of California, 1156 High Street, Santa Cruz, California 95064, United States

[b] School of Chemistry and Chemical Engineering, Jiangsu University, Zhenjiang, Jiangsu 212013, China

[c] School of Engineering, University of California, 5200 North Lake Road, Merced, California 95343, United States

[d] School of Environmental and Chemical Engineering, Jiangsu University of Science and Technology, Zhenjiang, Jiangsu 212003, China

[e] Department of Physics, University of California, 1156 High Street, Santa Cruz, California 95064, United States

* Email: shaowei@ucsc.edu

List of contents

- 23 Figures
- 8 tables

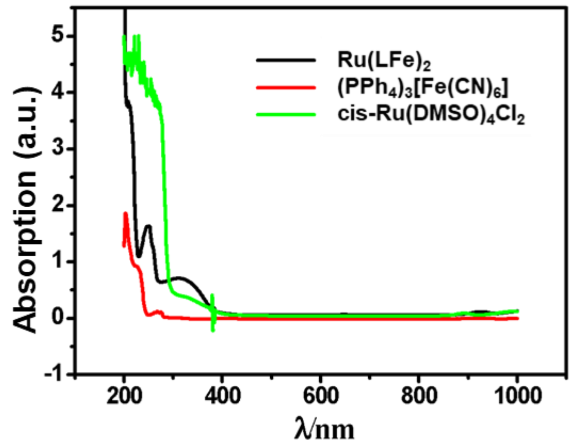

Fig. S1. UV-Vis spectra of $Ru(LFe)_2$, cis-$Ru(DMSO)_4Cl_2$, and $(PPh_4)_3[Fe(CN)_6]$.

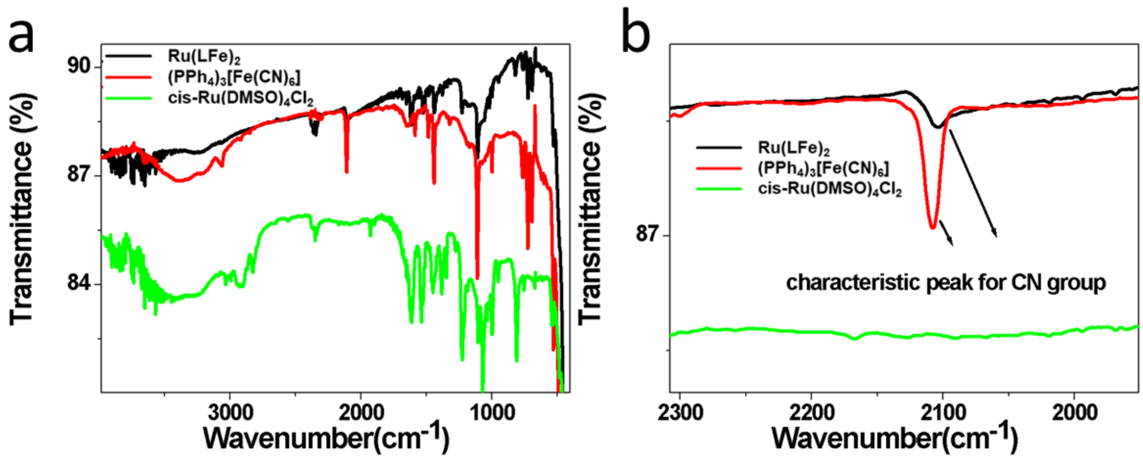

Fig. S2. (a) FTIR spectra of $Ru(LFe)_2$, cis-$Ru(DMSO)_4Cl_2$, and $(PPh_4)_3[Fe(CN)_6]$, and (b) the zoom in of the region between 2300 and 1950 cm^{-1}.

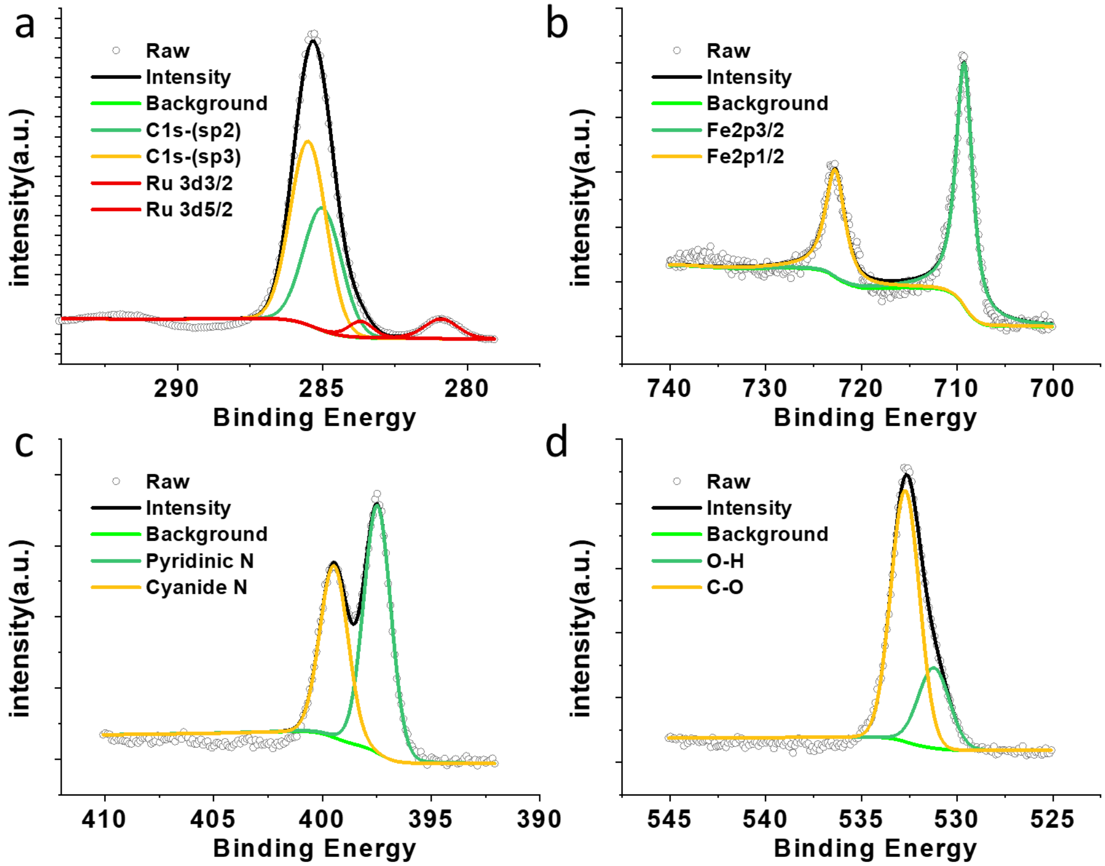

Fig. S3. High-resolution XPS scans of the (a) C 1s and Ru 3d, (b) Fe 2p, (c) N 1s and (d) O 1s electrons of the Ru(LFe)$_2$ complex. Black curves are experimental data and colored curves are deconvolution fits.

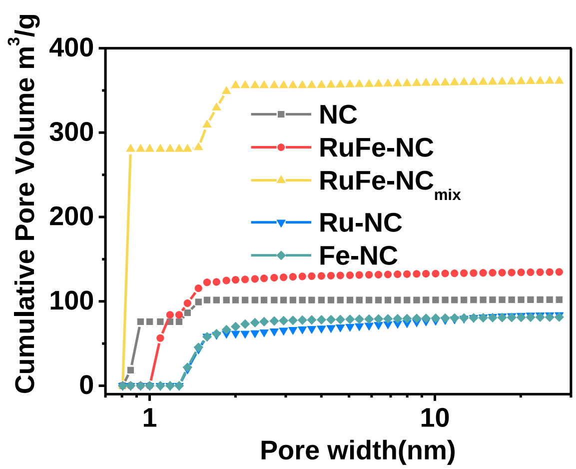

Fig. S4. Profiles of cumulative pore volume as the function of pore width of RuFe-NC, RuFe-NC$_{mix}$, Ru-NC, Fe-NC, and NC.

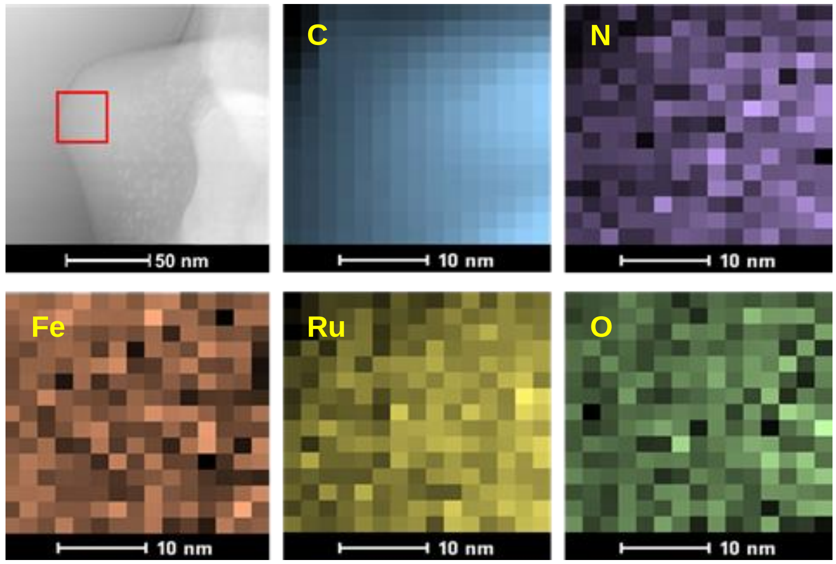

Fig. S5. Dark-field TEM image of RuFe-NC and the corresponding EELS elemental maps of the red box region: carbon (blue), nitrogen (purple), iron (orange), ruthenium (yellow), oxygen (green).

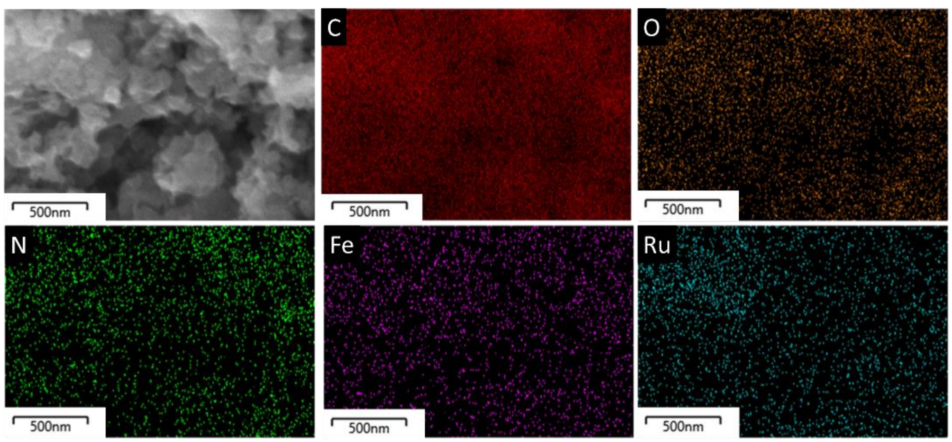

Fig. S6. SEM image and the corresponding EDS-based elemental maps of C, O, N, Fe, and Ru of RuFe-NC.

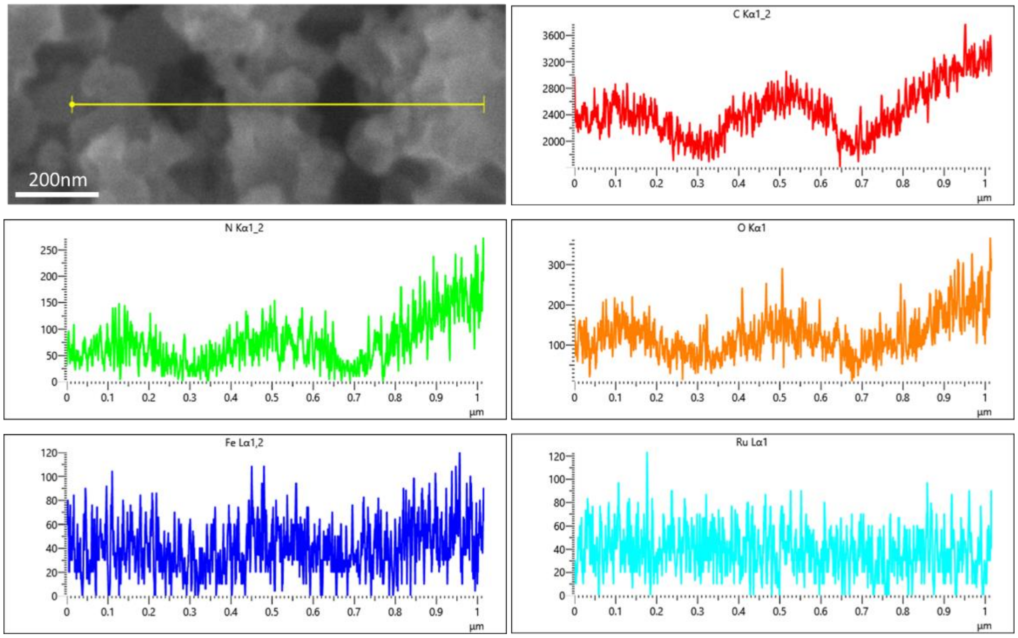

Fig. S7. SEM image and EDS line scans of the chemical composition of the RuFe-NC sample.

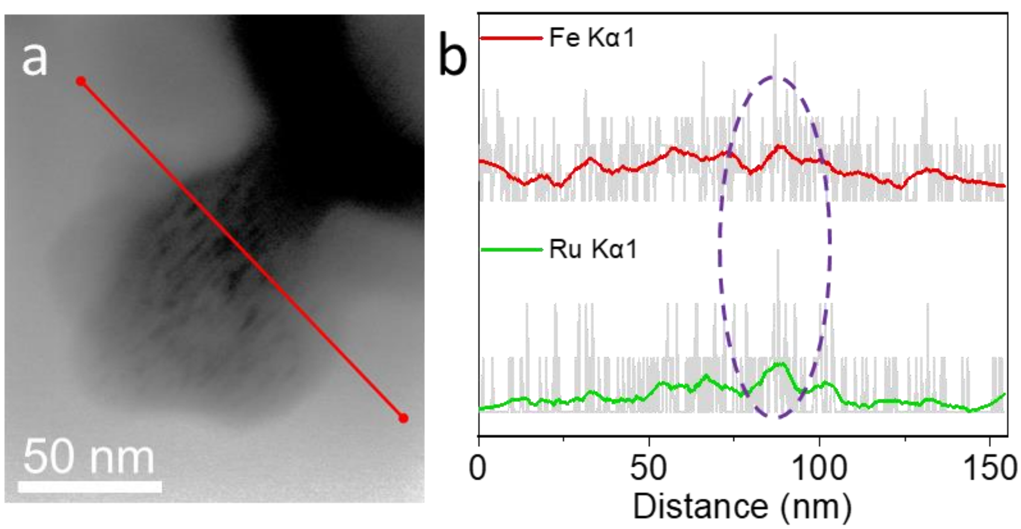

Fig. S8. (a) Representative TEM image of RuFe-NC. The red solid line represents the EDS line scan. (b) EDS line scan measurements of Fe and Ru. Note that gray curves are raw data, colored curves are smoothened results. Dashed purple circle highlights the concurrent increase of the Fe and Ru contents.

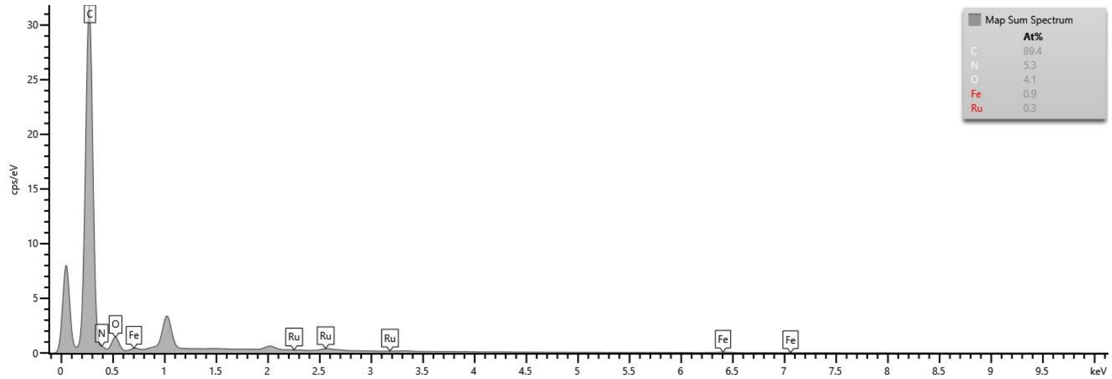

Fig. 9. EDS spectrum of RuFe-NC. Inset lists the elemental contents.

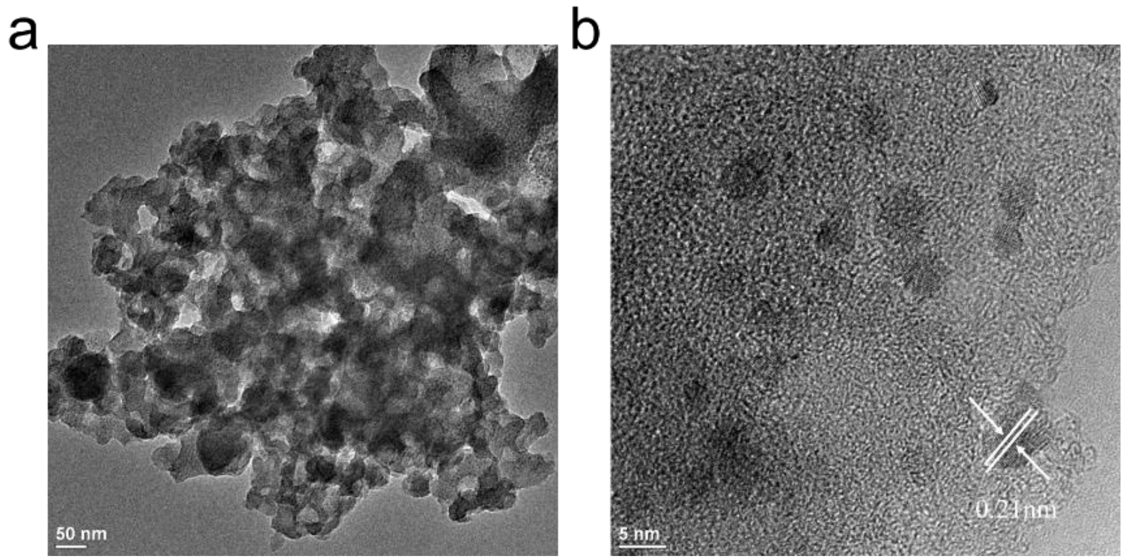

Fig. S10. Representative TEM images of Ru-NC at different magnifications. Scale bars are (a) 50 nm and (b) 5 nm.

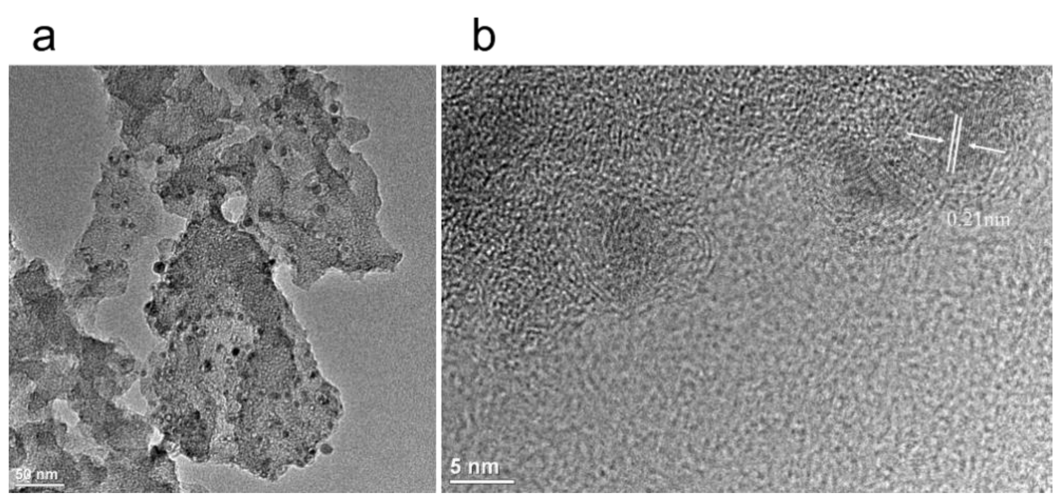

Fig. S11. Representative TEM images of Fe-NC at different magnifications. Scale bars are (a) 50 nm and (b) 5 nm.

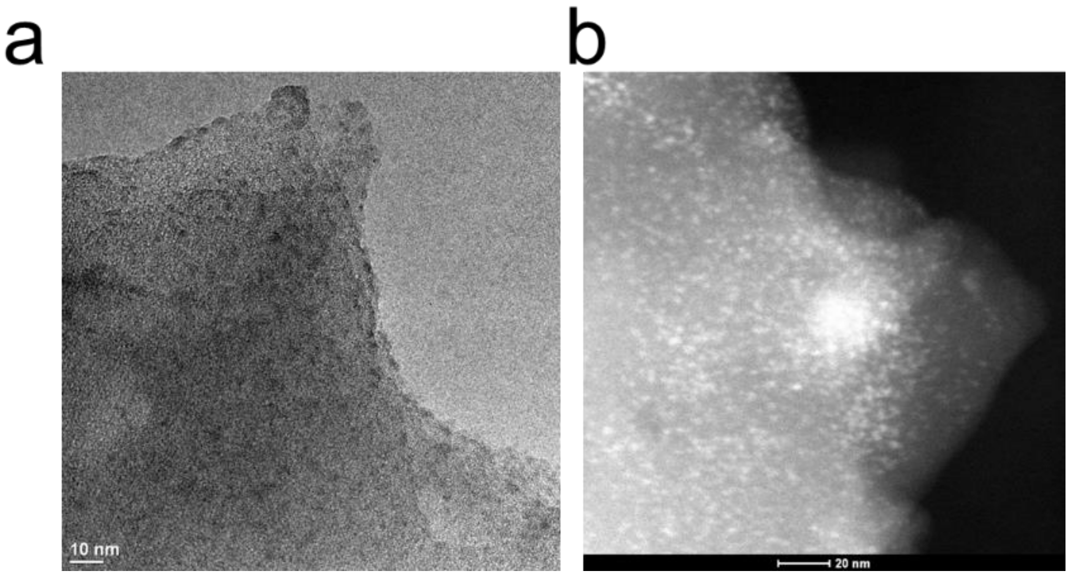

Fig. S12. (a) Bright-field and (b) dark-field TEM images of RuFe-NC$_{mix}$.

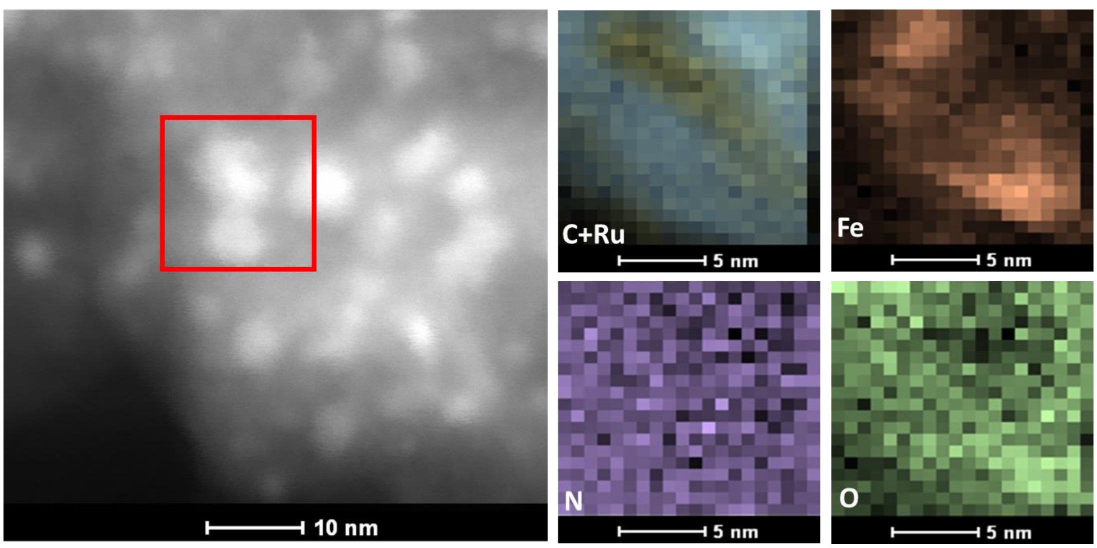

Fig. S13. (a) Representative dark-field TEM image of RuFe-NC$_{mix}$ and the corresponding elemental maps of C (blue), Ru (yellow), Fe (orange), N (purple), and O (green) in the red box region in panel (a).

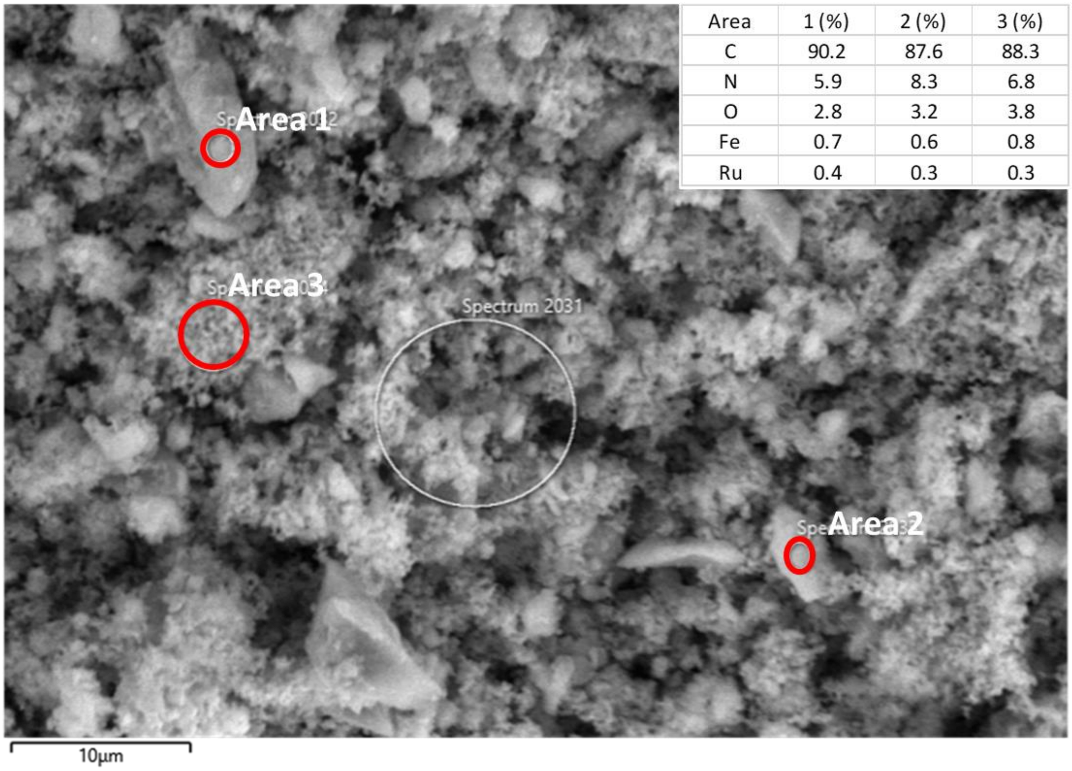

Area	1 (%)	2 (%)	3 (%)
C	90.2	87.6	88.3
N	5.9	8.3	6.8
O	2.8	3.2	3.8
Fe	0.7	0.6	0.8
Ru	0.4	0.3	0.3

Fig. S14. SEM image of RuFe-NC$_{mix}$ and the corresponding EDS survey of the elemental composition (inset table).

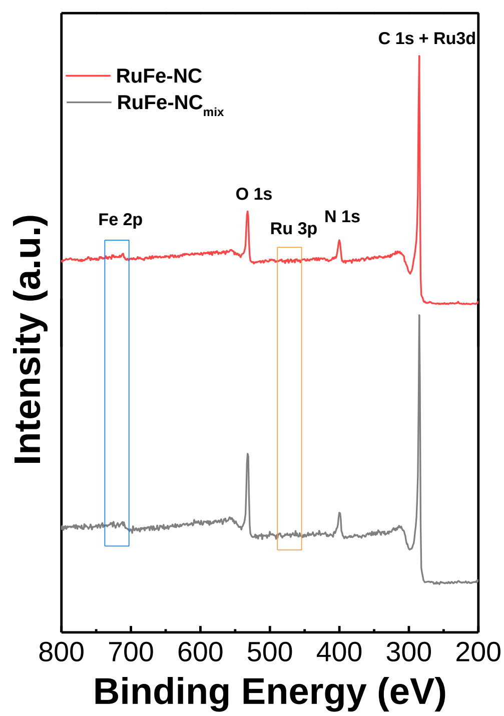

Fig. S15. XPS survey spectra of RuFe-NC and RuFe-NC$_{mix}$.

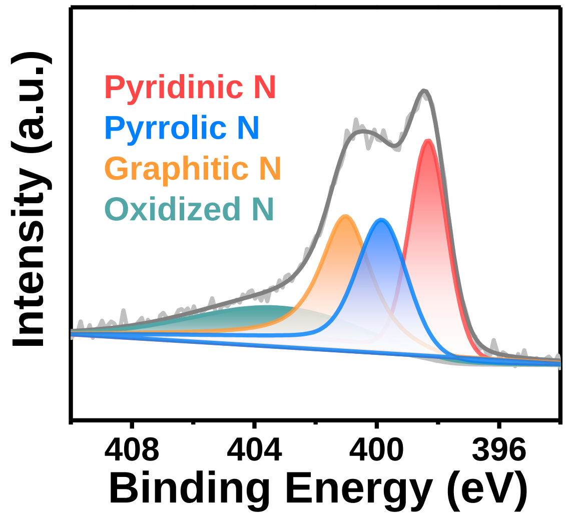

Fig. S16. High-resolution XPS spectrum of the N 1s electrons of RuFe-NC. Black curve is the experimental data and colored curves are deconvolution fits.

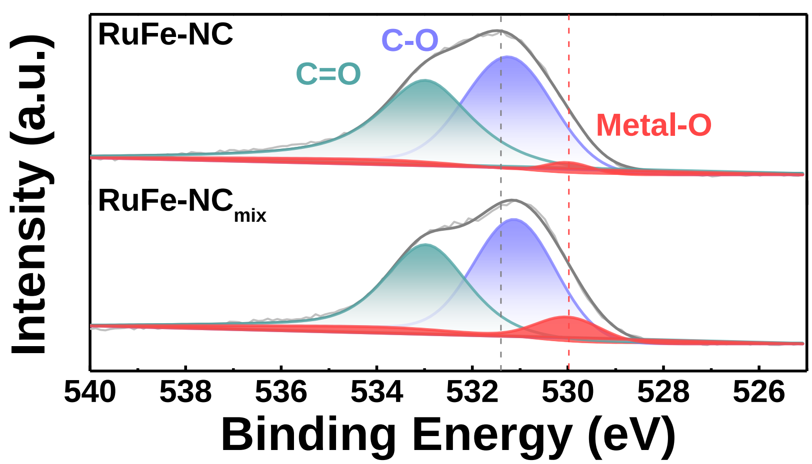

Fig. S17. High-resolution XPS spectra of the O 1s electrons of RuFe-NC and RuFe-NC-P. Black curves are the experimental data and colored curves are deconvolution fits.

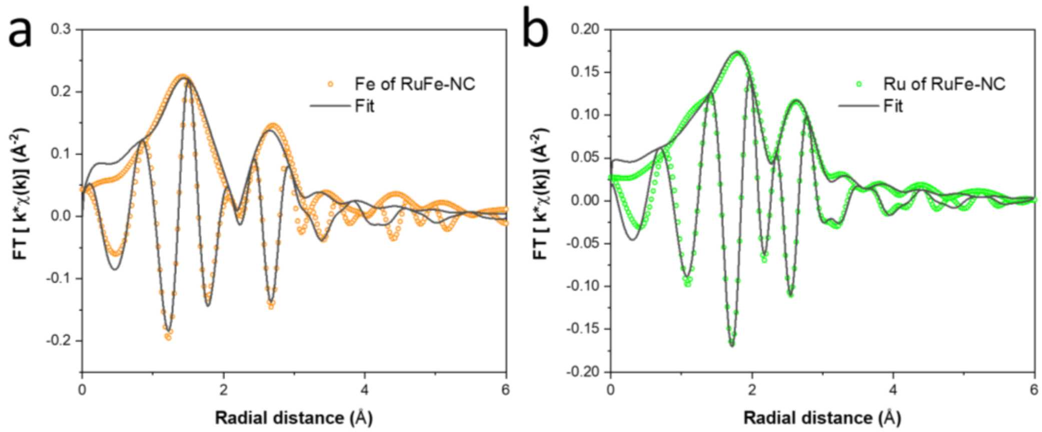

Fig. S18. Fitting results of the FT-EXAFS spectra of (a) Fe K edge and (b) Ru K edge of RuFe-NC. FFT range is 3.5 to 11 Å.

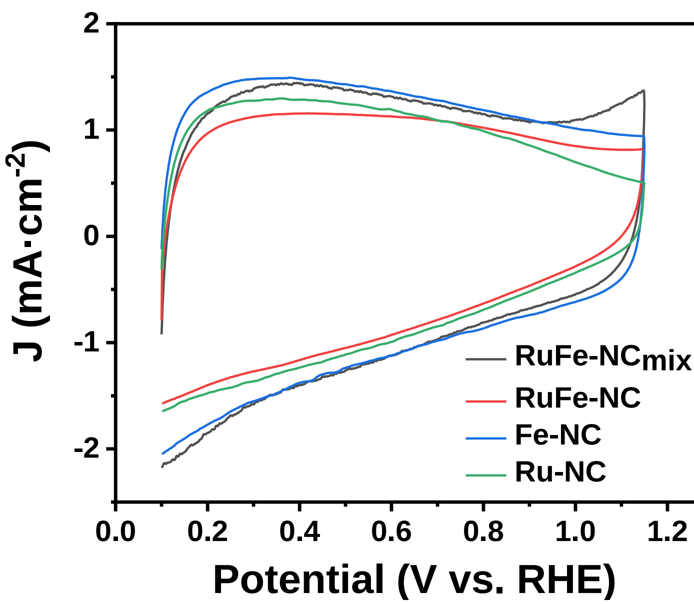

Fig. S19. CV measurements of RuFe-NC, RuFe-NC$_{mix}$, Fe-NC, and Ru-NC in N_2-saturated 0.1 M KOH at a scan rate of 50 mV s^{-1}.

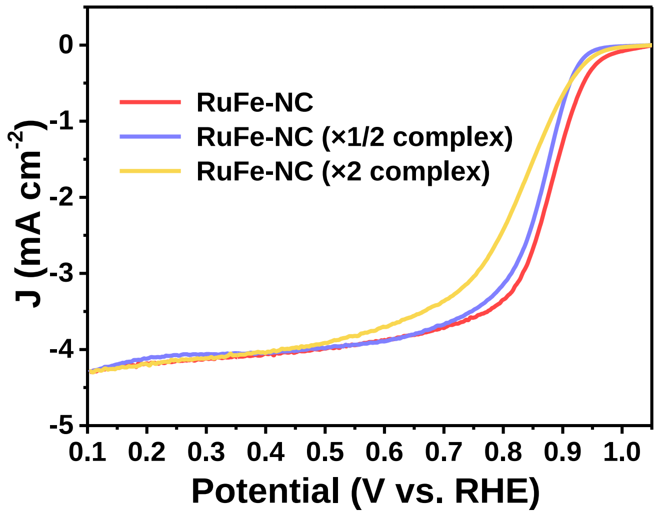

Fig. S20. ORR polarization curves of the RuFe-NC samples prepared at different $Ru(LFe)_2$ loadings at the rotation rate of 1600 rpm in O_2 saturated 0.1 M KOH.

Two additional RuFe-NC samples were prepared, one with the feeding ratio of RuFe complex to ZIF-8 reduced by half, RuFe-NC (x1/2 complex), and the other doubled, RuFe-NC (x2 complex). From Fig. S20, one can see that the LSV curves of both samples actually shifted cathodically as compared to that of RuFe-NC, suggesting that RuFe-NC represented the optimal composition for ORR.

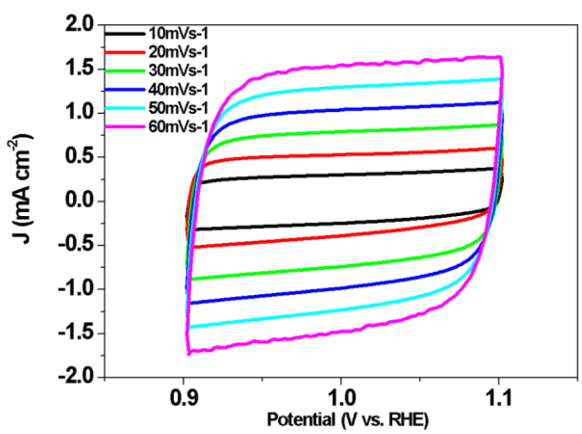

Fig. S21. Cyclic voltammograms of RuFe-NC in 0.1 M KOH within the potential range of +0.9 to +1.1V where no faradaic reaction occurs at difference scan rates.

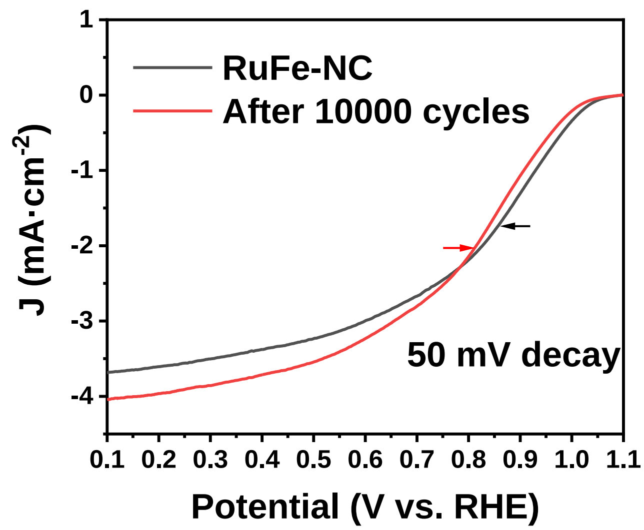

Fig. S22. LSV curves of RuFe-NC at a scan rate of 10 mV s^{-1} and a rotation speed of 1600 rpm in O_2 saturated 0.1 M KOH before and after stability tests of 10000 cycles in N_2-saturated 0.1 M KOH.

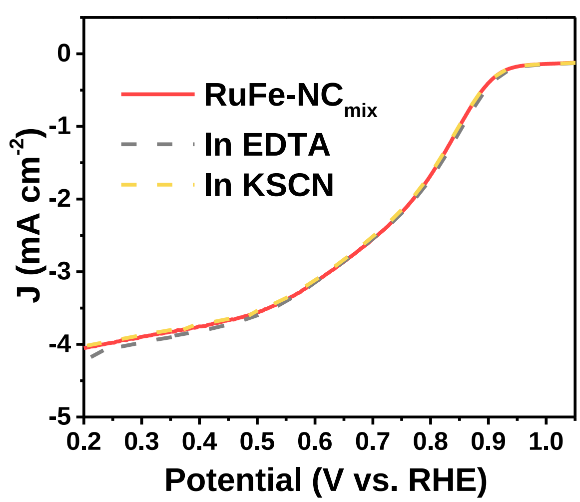

Fig. S23. Poisoning test of RuFe-NC_{mix} with EDTA and KSCN treatments.

Table S1. Detailed data of XPS devolution and calculations of RuFe-NC.

Elements	Types	Positions (eV)	Percentage (at%)	Percentage (at%)	Percentage (wt%)
C 1s	Sp2 C	284.63	38.893	84.241	79.438
	Sp3 C	285.69	24.706		
	C=O/N	288.80	20.682		
N 1s	Pyridinic N	398.30	2.036	6.917	7.610
	Pyrrolic N	399.68	1.672		
	Graphitic N	400.82	2.03		
	Oxidized N	403.36	1.176		
O 1s	C-O	531.23	3.962	8.329	10.473
	C=O	532.97	4.164		
	Metal-O	530.00	0.204		
Fe 2p	2p 3/2	711.51	0.199	0.448	1.973
	Satellite	717.57	0.010		
	2p 1/2	724.61	0.010		
	Satellite	730.67	0.005		
Ru 3d	3d 3/2	280.31	0.038	0.064	0.506
	3d 5/2	284.51	0.025		

Table S2. Detailed data of XPS devolution and calculations of RuFe-NC$_{mix}$.

Elements	Types	Positions (eV)	Percentage (at%)	Percentage (at%)	Percentage (wt%)
C 1s	Sp2 C	284.50	37.925	81.168	75.722
	Sp3 C	285.57	23.401		
	C=O/N	288.36	19.842		
N 1s	Pyridinic N	398.17	1.604	7.146	7.778
	Pyrrolic N	399.40	1.427		
	Graphitic N	400.77	2.363		
	Oxidized N	403.74	1.752		
O 1s	C-O	531.10	5.459	11.103	13.811
	C=O	532.96	4.722		
	Metal-O	530.00	0.921		
Fe 2p	Fe^0 2p 3/2	706.89	0.045	0.593	2.351
	Fe^{3+} 2p 3/2	711.26	0.224		
	Satellite	715.94	0.126		
	Fe^0 2p 1/2	719.99	0.023		
	Fe^{3+} 2p1/2	724.36	0.112		
	Satellite	729.04	0.063		
Ru 3d	3d 3/2	280.28	0.026	0.043	0.338
	3d 5/2	284.48	0.017		

Table S3. Detailed data of XPS devolution and calculations of NC.

Elements	Types	Positions (eV)	Percentage (at%)	Percentage (at%)	Percentage (wt%)
C 1s	Sp2 C	284.60	23.884	80.204	76.407
	Sp3 C	285.36	32.189		
	C=O/N	287.65	24.130		
N 1s	Pyridinic N	398.41	4.309	9.776	10.865
	Pyrrolic N	399.57	2.154		
	Graphitic N	400.95	2.548		
	Oxidized N	403.30	0.765		
O 1s	C-O	531.41	3.713	10.020	12.727
	C=O	532.93	6.306		

Table S4. Detailed data of XPS devolution and calculations of Ru-NC.

Elements	Types	Positions (eV)	Percentage (at%)	Percentage (at%)	Percentage (wt%)
C 1s	Sp2 C	284.63	37.712	83.658	80.305
	Sp3 C	285.71	26.381		
	C=O/N	288.44	19.565		
N 1s	Pyridinic N	398.21	2.311	9.050	10.135
	Pyrrolic N	398.91	1.931		
	Graphitic N	400.6	2.816		
	Oxidized N	401.82	1.992		
O 1s	C-O	531.07	3.187	7.258	9.290
	C=O	532.90	4.071		
Ru 3d	3d 3/2	280.45	0.020	0.033	0.271
	3d 5/2	284.65	0.013		

Table S5. Detailed data of XPS devolution and calculations of Fe-NC.

Elements	Types	Positions (eV)	Percentage (at%)	Percentage (at%)	Percentage (wt%)
C 1s	Sp2 C	284.69	29.500	78.704	73.587
	Sp3 C	285.70	29.162		
	C=O/N	288.99	20.041		
N 1s	Pyridinic N	398.45	4.747	10.007	10.916
	Pyrrolic N	399.88	1.450		
	Graphitic N	401.06	2.420		
	Oxidized N	403.30	1.389		
O 1s	C-O	531.14	32.156	10.833	13.505
	C=O	532.77	66.261		
	Metal-O	530.00	1.583		
Fe 2p	2p 3/2	711.31	0.097	0.457	1.992
	Satellite	716.84	0.069		
	2p 1/2	724.41	0.236		
	Satellite	729.94	0.035		

Table S6. Fe and Ru contents of the sample series

Sample	Theoretical values (wt%)		XPS values (wt%)		ICP values (wt%)	
	Fe	Ru	Fe	Ru	Fe	Ru
$Ru(LFe)_2$ complex	4.50%	4.00%	4.05%	4.43%		
RuFe-NC	1.30%	1.20%	1.97%	0.50%	1.69%	0.0026%
RuFe-NC(x1/2)	0.70%	0.60%			1.14%	0.0019%
RuFe-NC(x2)	2.60%	2.40%			3.07%	0.0089%
RuFe-NC_{mix}	1.30%	1.20%	2.35%	0.33%	2.64%	0.0059%
Ru-NC		1.20%		0.27%		0.0026%
Fe-NC	1.30%		1.99%		1.91%	

Table S7. Fitting results of XAS for RuFe-NC.

Bond	Bond Length (Å)	Coordination Number	R^2
Fe-O	1.999	4.81	0.099
Fe-Fe	2.950	2.00	
Bond	**Bond Length (Å)**	**Coordination number**	**R^2**
Ru-O	2.044	2.50	0.06
Ru-P	2.289	1.85	
Ru-Fe	2.987	1.16	
Ru-Ru	2.742	0.62	
Ru-Fe	3.882	1.74	

Tables S8. Comparison of catalyst performance with relevant materials in the literature.

Sample	Precursors	$E_{1/2}$ (V vs. RHE)	n	Stability	Reference
RuFe-NC	Trinuclear complex/ZIF8	+0.87	3.98 @ +0.8 V vs. RHE	negligible change after 5K CVs, 40 mV after 10K CVs.	This work
Fe_2O_3@NC&bio-C-800	$FeCl_3$ and pyrrole	+0.85	4.0 @ +0.2 V vs. RHE	91% retention of current density after 10000s	J. Energy Chem., 2020, 44, 121-130
Fe_2O_3/KB	$Fe(NO_3)_3$ and Ketjen Black	+0.7	3.7 @ +0.2 V vs. RHE	42 mV decay after 21K CVs	ACS Appl. Mater. Interfaces, 2021, 13, 44195-44206
γ- Fe_2O_3@CNFs-12	$FeSO_4$ and Pt/C	+0.905	3.5-4.0	5 mV after 5K CVs	Chem. Eng. J., 2021, 415, 129033
Fe_2O_3-MoO_3/NG	$FeCl_3$/$(NH_4)_6Mo_7O_{24}$/ GO/Melamine	+0.82	3.8	15 mV after 2K CVs	Chem. Eng. J., 2021, 410, 128358
α- Fe_2O_3/A-C3N4	$FeCl_4$/1-Butyl-3-methylimidazolium chloride	+0.6	3.7	86% retention of current density after 10000s	J. Mater. Sci., 2022, 57, 2012-2020
Fe_2O_3/N-PCs-850/GC	$FeCl_3$/mulberry leaves	+0.8	3.9	76.8% retention after 3000s	Catalysts, 2018, 8, 101
GF+N_2+Fe1_800	$FeCl_3$/GO	+0.84	4 @ +0.65 V vs. RHE	96.2% retention after 20h	ACS Catal., 2016, 6, 3558-3568
$LaMn_xFe_{1-x}O_3$	$La(NO_3)_3$/ $Fe(NO_3)_3$/ Mn(NO3)2	+0.7	3.87 @ +0.3-0.5 V vs .RHE	88.1% retention after 10000s	Front. Mater. Sci., 2020, 14, 459-468
CoNP@bio-C-a	$Co(OH)_2$/$NaH_2PO_2{\cdot}H_2O$/CC powder	+0.85	4 @ +0.4-0.5 V vs. RHE	73% retention after 10000s	RSC Adv., 2022, 12, 207-215
MnO_2/C	$Mn(NO_3)_2$	+0.75	Not provided	~50 mV decay after 1K CVs	ACS Catal., 2015, 5, 4825-4832